Palaeogeography, Palaeoclimatology, Palaeoecology 589 (2022) 110844

Contents lists available at ScienceDirect

Palaeogeography, Palaeoclimatology, Palaeoecology

journal homepage: www.elsevier.com/locate/palaeo

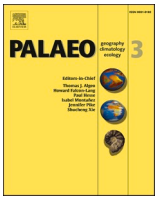

# Monsoon-related changes in surface hydrography and productivity in the Bay of Bengal over the last 45 kyr BP

Komal Verma [a], Arun Deo Singh [a,b,*], Pradyumna Singh [a,b], Harshit Singh [a], Rajeev Kumar Satpathy [a], Prem Raj Uddandam [a], Pothuri Divakar Naidu [c]

[a] Department of Geology, Banaras Hindu University, Varanasi 221005, India
[b] DST-Mahamana Centre of Excellence in Climate Change Research, Institute of Environmental and Sustainable Development, Banaras Hindu University, Varanasi 221005, India
[c] Formerly at CSIR-National Institute of Oceanography, Dona Paula, Goa 403004, India

ARTICLE INFO

Editor: Howard Falcon-Lang

*Keywords:*
Planktic foraminifera
Mixed-layer
Salinity stratification
Winter mixing
Pleistocene
Holocene

ABSTRACT

Temporal variations of mixed-layer planktic foraminiferal abundances in a sediment core from the western Bay of Bengal (off Krishna – Godavari Basin) are used to reconstruct surface hydrographic structure and productivity in response to the changes in seasonal monsoon precipitation and wind intensity over the last 45 kyr BP. The faunal proxy records (abundances of eutrophic and oligotrophic species/group and *G. bulloides / G. ruber* ratio) exhibit millennial-scale variations during the late Glacial, deglacial and Holocene periods. Our results show that the surface hydrographic conditions and productivity varied in concert with the Northern Hemisphere climatic events (Dansgaard-Oeschger (D—O) oscillations and Heinrich (H) events). The productivity in the late Glacial period between 44 and 19 kyr BP in general was higher compared to the deglacial and Holocene. Within the late Glacial period, we record high productivity during the cold phases of the D—O cycles (43–41, 35–34, 28.5–28, 27–25 kyr BP), North Atlantic Heinrich events (39.5–38.5 kyr BP, H4; 31.5–30 kyr BP, H3; 24–23 kyr BP, H2) and during the Last Glacial Maximum (22–19 kyr BP). These productivity maxima are related to the pronounced advection of nutrient-rich subsurface waters to the euphotic zone induced by the intensified Northeast (NE) Monsoon winds in non-stratified/weakly stratified surface ocean conditions due to reduced Southwest (SW) Monsoon precipitation and freshwater influx. Our faunal record suggests a major reorganization of seasonal monsoon wind circulations after 16 kyr BP, when the SW monsoon intensified and concomitantly the NE monsoon weakened. Enhanced SW monsoon precipitation and freshwater flux to the Bay of Bengal between 15 and 13 kyr BP, a period broadly corresponding to the warm Bølling-Allerød (B/A) event, resulted in strong stratification of mixed-layer water and oligotrophic conditions. An increase in productivity between 13 and 11 kyr BP (equivalent to the cold Younger Dryas (YD) event) is attributed to intensified mixing of weakly stratified mixed layer waters by NE monsoon winds. During the early Holocene between 9 and 6 kyr BP, intensified SW monsoon precipitation and high fluvial discharge resulted in strongly stratified, nutrient-poor waters in the mixed-layer and a conspicuous reduction in productivity. However, a moderate increase in productivity is recorded between 5 and 3 kyr BP, when the SW monsoon intensity and associated fluvial discharge gradually declined and ocean surface stratification weakened resulting in conditions favourable for NE monsoon winds induced mixing. Overall, our results show that the alternating periods of intensified SW monsoon precipitation and NE monsoon wind circulation modulated the surface hydrographic structure and productivity patterns in the Bay of Bengal.

## 1. Introduction

The surface hydrography of the Bay of Bengal (BoB) is modulated by the seasonally reversing monsoonal wind patterns. The excessive freshening due to in situ precipitation and enormous fluvial discharge from the Himalayas and peninsular India by major rivers (Ganga, Brahmaputra, Irrawaddy, Krishna, Godavari, Mahanadi) causes a strong surface water stratification in the BoB (Sengupta et al., 2006; Prasanna

* Corresponding author at: Department of Geology, Banaras Hindu University, Varanasi 221005, India.
*E-mail address:* arundeosingh@yahoo.com (A.D. Singh).

https://doi.org/10.1016/j.palaeo.2022.110844
Received 3 October 2020; Received in revised form 11 January 2022; Accepted 11 January 2022
Available online 21 January 2022

Kumar et al., 2010). The northern BoB receives maximum freshwater flux during the SW monsoon (Ittekkot et al., 1991), therefore this region is fresher than the southern BoB (Subramanian, 1996). The strongly stratified surface waters of the BoB substantially decreases biological productivity in this basin (Prasanna Kumar et al., 2002, 2007), unlike the Arabian Sea, where SW monsoon winds induce strong upwelling in its western sector and NE winds-related convective mixing in the north-eastern sector results in an overall high primary productivity (Banse, 1987; Prell et al., 1990; Madhupratap et al., 1996). The wind-driven vertical mixing and/or upwelling, responsible for transporting nutrients from subsurface waters into the euphotic zone leading to phytoplankton productivity, is relatively weaker in the BoB due to its year-round stratified surface ocean conditions (Balachandran et al., 2008). Therefore, the intensity of monsoonal precipitation and freshwater influx to the bay strongly modulate the biological productivity in the BoB. Additionally, local hydrographic processes associated with the seasonal development of cyclonic gyre and eddies significantly influence the surface hydrography and seasonal productivity pattern (Gomes et al., 2016). Hence, the paleoproductivity record from this region would provide useful insights into the past changes in surface hydrographic conditions induced by the seasonal monsoon variability.

Planktic foraminifera respond rapidly to changes in surface hydrography (salinity, temperature and nutrient conditions of mixed-layer), as reflected by variations in the abundances of species and chemical composition of their tests (e.g., Kroon et al., 1990; Peeters and Brummer, 2002; Ivanova et al., 2003; Anand et al., 2008; Singh et al., 2011, 2018). Therefore, planktic foraminiferal assemblages in the sedimentary record of the BoB have great potential to reconstruct past changes in surface water stratification, mixed-layer environment and productivity, which are tightly coupled with seasonally reversing Indian monsoon winds and surface ocean circulation.

Previous paleoceanographic reconstructions in the Arabian Sea employing foraminiferal assemblages provided deep insights into the understanding of seasonal Indian monsoon variability and associated changes in upper water column structure on long to short-term time scales (e.g., Clemens et al., 1991; Naidu and Malmgren, 1996; Vénec-Peyré and Caulet, 2000; Singh et al., 2006, 2011; Satpathy et al., 2019). In recent years, a series of sedimentological, geochemical and isotope proxy records from the late Quaternary sediments of the BoB have also been developed to reconstruct the Indian summer monsoon driven changes in precipitation, continental runoff, sediment provenance and erosional history of source region (e.g., Kudrass et al., 2001; Pattan et al., 2013; Sijinkumar et al., 2016; Joussain et al., 2016; Da Silva et al., 2017; Weber and Reilly, 2018; Weber et al., 2018; Prajith et al., 2018; Nilsson-Kerr et al., 2019; Ota et al., 2019; Li et al., 2019). Studies based on the paired oxygen isotope and Mg/Ca measurements of surface dwelling foraminifera provided useful records of past changes in sea-surface salinity (SSS) and sea-surface temperature (SST) in the BoB driven by the SW monsoon (Kudrass et al., 2001; Govil and Naidu, 2011; Rashid et al., 2011; Raza et al., 2014). Earlier studies have also shown that the SW monsoon induced salinity stratification strongly controlled past productivity variations in the bay (e.g., Pattan et al., 2013; Da Silva et al., 2017; Zhou et al., 2020). However, our understanding of the evolution of biological productivity in the BoB and its relation to the changes in upper water column structure in response to the seasonal monsoon (summer SW and winter NE) wind circulation and precipitation remains incomplete. In this study, we provide the first high resolution record of planktic foraminiferal assemblage changes in a sediment core of western BoB (off Krishna – Godavari Basin). Based on our foraminiferal proxy records, we aim to document changes in upper water column structure (surface water stratification, mixed-layer depth and nutrient condition) in response to the variation in summer and winter monsoon strengths on glacial/interglacial and millennial timescales. We also evaluate the influence of monsoon induced surface hydrographic conditions on the productivity over the last 45 kyr BP, to gain insight into the relationship between Indian monsoon dynamics and evolution of productivity in the western BoB.

## 2. Oceanographic setting

The Bay of Bengal, a semi-enclosed basin in the north-eastern Indian Ocean is forced by the seasonally reversing monsoon winds. The winds in the equatorial Indian Ocean also affect surface circulation pattern in the BoB (Hastenrath and Greischar, 1989; McCreary et al., 1993; Vinayachandran et al., 2002). The seasonal monsoon cycle not only influences the surface hydrography but also affects the sediment flux to the bay (Ramaswamy and Nair, 1994; Guptha et al., 1997; Stoll et al., 2007). During the SW monsoon season (June–September), the strong southwesterly winds drive moisture-laden maritime air into the BoB (Narvekar and Prasanna Kumar, 2006). Enormous freshwater discharge from major rivers and excess of precipitation over evaporation during this season cause stratification of surface waters, which is more pronounced in the northern BoB.

The annual mean SSS in the BoB is lowest (~ 29 psu) in its northern sector north of 20° N and SSS increases southward reaching to ~34 psu around 7° N (Murty et al., 1992). The BoB experiences a large seasonal variability in SSS (Prasanna Kumar et al., 2002; Sarma et al., 2013). Maximum seasonal SSS variability (>3 psu) is recorded in the northern BoB dominated by surface water freshening in SW monsoon and post-monsoon season (Sarma et al., 2013). However, in the southern region, the seasonal SSS variation is reported to be about 1 psu with a minimum during early winter (November – December) attributed to the NE monsoon precipitation over southeastern India (Dimri et al., 2016). The annual mean SST varies between ~27 °C in the north and ~ 29 °C in the southern BoB with a meridional difference of 1.5 °C. A gradual increase of SST is noticed from February to June with its maximum in April, whereas a rapid surface cooling occurs north of 13° N from November to February (Narvekar and Prasanna Kumar, 2006).

High precipitation and fluvial runoff during SW monsoon create a large low-salinity plume in the bay resulting in surface water stratification. The salinity stratification promotes upper water column stability and a shallow mixed-layer depth (~ 5 to 30 m) [Narvekar and Prasanna Kumar, 2014]. In general, the mixed-layer depth (MLD) is deeper south of 15° N than in the northern BoB during June–September and November–February. The stratified waters prevent the transport of nutrients from subsurface waters across the euphotic zone leading to the low primary productivity and oligotrophic conditions. Unlike the Arabian Sea, there is no evidence of strong upwelling in the BoB during summer except for a narrow band close to the southwestern boundary (Shetye et al., 1991; Kumar et al., 2004). Nevertheless, the cyclonic gyre promotes upwelling of nutrient rich deeper waters into the euphotic zone and winter phytoplankton bloom in the western BoB south of 20° N (Vinayachandran and Yamagata, 1998; Unger et al., 2003; Gomes et al., 2016).

## 3. Material and methods

A 8.2 m long gravity core (SK 218/1) was collected from a water depth of 3307 m off Krishna – Godavari Basin (14°02′06″ N, 82°00′12″ E), from the western BoB by the ORV *Sagar Kanya* in 2005 (Fig. 1). The core provides a continuous, undisturbed, turbidite-free sediment record, thus suitable for paleoceanographic reconstruction (Govil and Naidu, 2011). The age model is based on 8 AMS $^{14}$C dates (Table 1) and correlation of the $\delta^{18}$O record of *Globigerinoides ruber* with the $\delta^{18}O_c$ global isostack curve of Martinson et al. (1987) [Naidu and Govil, 2010; Govil and Naidu, 2011]. The oxygen isotope record ($\delta^{18}$O *G. ruber*) of the last 32 kyr BP (Naidu and Govil, 2010) is extended in this study to 45 kyr BP (Fig. 3). The oxygen isotope measurements for the entire core were carried out at Bremen University, Germany and the details are given in Naidu and Govil (2010).

In total, 158 sediment samples at regular intervals of 2 to 4 cm were taken for foraminiferal studies. For separation of foraminiferal tests,

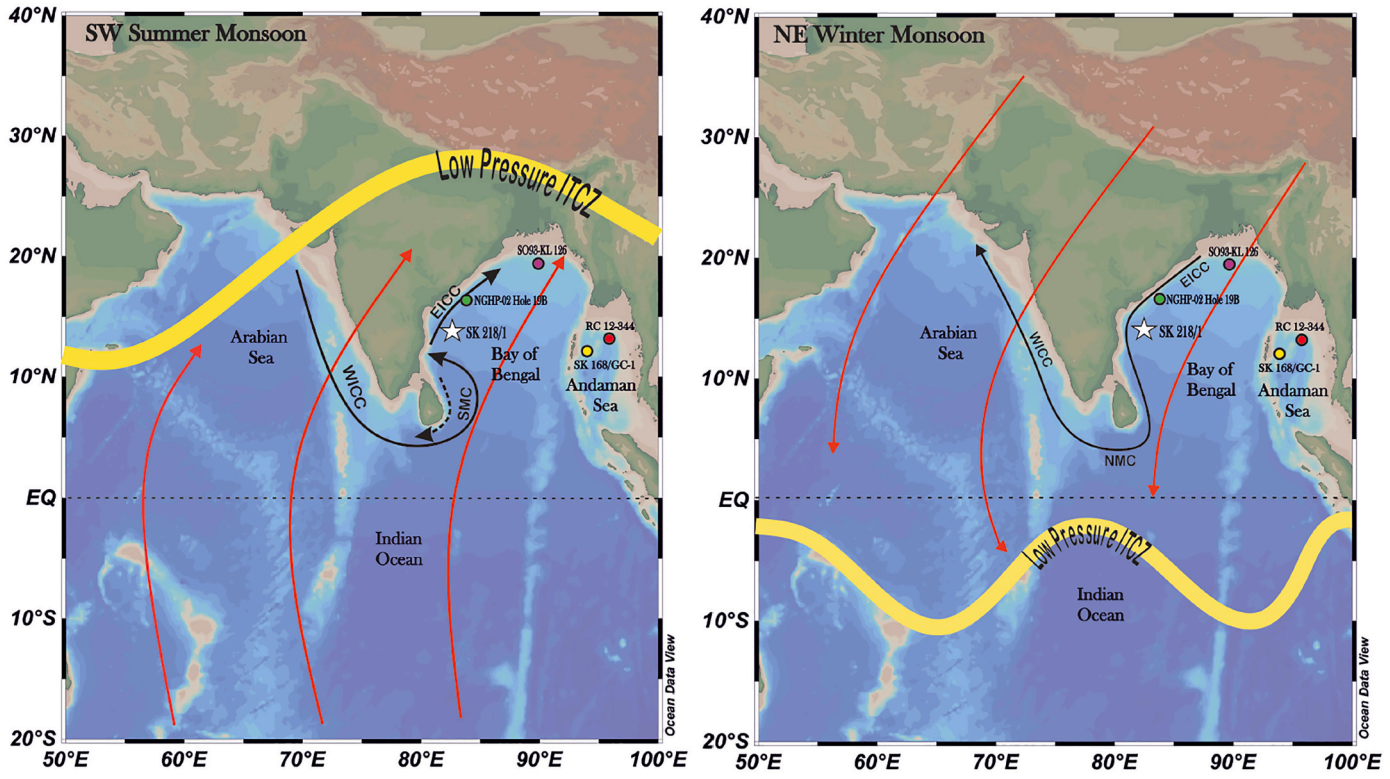


**Fig. 1.** Map showing the location of core SK 218/1 (white star; this study) in the Bay of Bengal and other core sites discussed in the text (SO93-KL 126, violet circle, northern Bay of Bengal; NGHP-02 Hole 19B, green circle, western Bay of Bengal; RC 12–344, red circle and SK 168/GC-1, yellow circle, northern Andaman Sea). Schematic representation of dominant wind directions (red lines) and coastal currents (black lines) during the SW and NE monsoon seasons (after Schott and McCreary, 2001). Seasonal position of Inter Tropical Convergence Zone (ITCZ) is denoted by yellow line (after Zorzi et al., 2015). (Base map generated from Ocean Data View software version 4.7.10; Schlitzer, 2014). WICC: West Indian Coastal Current; EICC: East Indian Coastal Current; SMC: Southwest Monsoon Current; NMC: Northeast Monsoon Current. (For interpretation of the references to colour in this figure legend, the reader is referred to the web version of this article.)

**Table 1**
AMS $^{14}$C dates and calibrated ages (in calendar years before present) for core SK 218/1 (Govil and Naidu, 2011). The AMS radiocarbon dates measured on monospecific samples of *Globigerinoides ruber* were converted to calendar ages by using CALIB 6.0 (Stuiver and Reimer, 1993) and considering a reservoir age of 400 years (Southon et al., 2002).

| S. No. | Lab reference No. | Material | Depth (cm) | $^{14}$C ages (yr BP) | Calibrated calendar age (yr) |
|---|---|---|---|---|---|
| 1 | KIA2845–5 | *G. ruber* | 68 | 1055 ± 30 | 300 |
| 2 | AAS93880 | *G. ruber* | 150 | 3840 ± 100 | 3311 |
| 3 | KIA2844–8 | *G. ruber* | 266 | 10,400 ± 60 | 10,976 |
| 4 | KIA2844–7 | *G. ruber* | 322 | 13,940 ± 90 | 15,948 |
| 5 | AAS93881 | *G. ruber* | 350 | 16,410 ± 100 | 18,772 |
| 6 | AAS93883 | *G. ruber* | 498 | 22,100 ± 410 | 25,478 |
| 7 | AAS93884 | *G. ruber* | 550 | 29,300 ± 330 | 32,822 |
| 8 | KIA2844–6 | *G. ruber* | 638 | 33,060 ± 780 | 36,884 |

sediment samples were processed following standard micropaleontological techniques (Singh et al., 2018). Census counts of planktic and benthic foraminifera were made on the >125 μm size fraction. Based on census data, percentage abundance of each planktic foraminiferal species was calculated. The taxonomic classification of planktic foraminiferal species is based on Kennett and Srinivasan (1983), Hemleben et al. (1989), Spezzaferri et al. (2015) and Poole and Wade (2019). We also used previously published $\delta^{18}O_{sw}$ record of the same core (Govil and Naidu, 2011) as supporting evidence for our foraminiferal assemblage based paleoceanographic inferences.

## 4. Results

### 4.1. Planktic foraminiferal assemblage

In total, 30 planktic species were recorded, including both surface dwelling mixed-layer and deep dwelling thermocline species. *Globigerinita glutinata, Globigerinoides ruber* and *Globigerina bulloides* are the most abundant surface dwelling mixed-layer species. Other common mixed-layer species are *Globigerina falconensis, Trilobatus quadrilobatus, Trilobatus trilobus* and *Trilobatus sacculifer*. *Globorotalia menardii* and *Neogloboquadrina dutertrei* are the thermocline species with frequent occurrences in the core. Following the taxonomic concept of Poole and Wade (2019), we considered *T. trilobus, T. quadrilobatus* and *T. sacculifer* as morphospecies of *T. sacculifer* plexus, hence we combined them together for the present study. We utilize abundance records of mixed-layer planktic foraminifera for paleoceanographic reconstruction, as these species respond strongly to changes in surface hydrographic conditions (salinity stratification, mixed-layer depth and nutrient condition) [Singh et al., 2011, 2018].

### 4.2. Evaluation of dissolution effects on foraminiferal census counts

Planktic foraminifera mainly feed on phytoplankton, hence they are strongly related to the primary productivity (e.g., Hemleben et al., 1989). However, factor other than productivity such as dissolution of calcareous tests may also influence the composition of fossil foraminiferal assemblages, thus altering the original microfaunal signatures of

past environmental conditions. In order to evaluate the effect of calcium carbonate dissolution on our foraminiferal assemblages, we determined dissolution indices; DI (dissolution index): number of dissolution resistant planktic foraminiferal tests / total specimens of common dissolution susceptible planktic foraminifera in 1 g × 10, after Berger (1973) and Ivanova et al. (2003); and benthic/planktic foraminiferal (B/P) abundance ratios: total number of benthic foraminiferal tests / total specimens of benthic + planktic foraminifera in 1 g, after Van der Zwaan et al. (1990) and Lübbers et al. (2019) [Fig. 2]. The DI record reflects that the values of dissolution resistant / susceptible species abundance ratio is <5.0 in the majority of the core samples except in 5 samples {22.6, 24, 29.4, 37.4 and 40.5 kyr BP} (Fig. 2). Low DI values are suggestive of minimal dissolution of planktic foraminiferal tests. B/P ratio shows that the planktic foraminiferal abundances are generally much higher than the benthic foraminiferal abundances, except during some intervals of MIS 2 and MIS 3 (28.9, 34.5 and 37.8 kyr BP) and since 1.5 kyr BP, when benthic foraminiferal abundances increased significantly (Fig. 2). Interestingly, abundances of dissolution susceptible planktic species remained high during these intervals of relatively high benthic foraminifera as evidenced by low DI values (Fig. 2). Therefore, the temporal variation of the B/P ratio is most likely related to changes in export production flux and not to the dissolution of planktic foraminiferal tests. However, we cannot rule out the effect of dissolution on foraminiferal tests during those very brief periods of high DI values corresponding to the sharp spikes of resistant species abundances (D1-D5) (Fig. 2). Each of these abundance spikes represents only a single sample having predominance of *N. dutertrei*, a species associated with nutrient-rich upper thermocline waters. However, with the present sample resolution it is not possible to ascertain, whether these spikes, besides the dissolution, are also related to the increased production of the resistant species *N. dutertrei*. Therefore, we assume that the pattern of variation in the planktic foraminiferal record except for those intervals discussed above (D1-D5) is not an artifact of carbonate dissolution, but represents true paleoceanographic events.

### 4.3. Temporal variation in planktic foraminiferal abundance

Temporal variation in relative abundances of planktic species in core SK 218/1 (Fig. 3) provides interesting clues for evaluating the changes in surface hydrography in the western BoB during the last 45 kyr BP. The species abundance records indicate pronounced variations during the late Glacial, the deglacial and Holocene periods. The late Glacial period between 44 and 19 kyr BP is characterized by high abundances of *G. bulloides*, *G. glutinata* and *G. falconensis*, as compared to the deglacial (between 19 and 11 kyr BP) and Holocene periods. However, *G. falconensis* is overall less abundant than the other two species. *G. falconensis* abundance broadly follows that of *G. bulloides*. The long-term abundance changes in these three species are superimposed by the millennial-scale variability, apparently more pronounced during the late Glacial (Fig. 3). The abundance of *G. bulloides* peaks during certain intervals between 44 and 19 kyr BP, then declines rapidly between 17.5 and 15 kyr BP (Fig. 3). Its abundance remained relatively low until 13.5 kyr BP and then increased between 13 and 11 kyr BP. The early part of the Holocene (9–6 kyr BP) is characterized by a low abundance of *G. bulloides*. *G. bulloides* abundance increased again between 5 and 3 kyr BP and since 1.5 kyr BP in the late Holocene. During the late Glacial period, prominent abundance maxima of *G. bulloides* occur during 42–41, 39–38, 27–25, 24–23, 22–19 kyr BP and at around 37, 35 and 33 kyr BP. *G. glutinata* shows its peak abundances during 43–41, 40–38, 35–33.5, 31–30, 24–23, 21–19 kyr BP and at around 36 kyr BP (Fig. 3). The oscillations in faunal abundance appear to be comparable with millennial-scale climatic events in Greenland ice cores (Fig. 3). It is apparent that despite minor differences in magnitude of variation and timing of peak abundances, *G. bulloides* and *G. glutinata* both show their abundance maxima during the periods corresponding to the Northern Hemisphere cold phases (Heinrich events 2–4 and Dansgaard-Oeschger (D—O) stadials). Given the sample resolution constraints, however, it is not possible to precisely record faunal changes during all D—O events and Heinrich event 1. Interestingly, the abundance of *G. glutinata* is conspicuously low between 13 and 11 kyr BP, a period corresponding to the cold Younger Dryas (YD) event, when *G. bulloides* and *G. falconensis* both show high abundances. After a prominent increase during 11–10 kyr BP, *G. glutinata* abundance declines between 9 and 6 kyr BP and increases again between 6 and 4 kyr BP. The *G. ruber* and *T. sacculifer* plexus remains less abundant and follows a similar pattern of variation prior to 16 kyr BP. Nevertheless, the pattern of abundance variation in the *T. sacculifer* plexus is generally opposite to that of *G. ruber* since 16 kyr BP. Interestingly, the *G. ruber* and *T. sacculifer* plexus does not show a distinct short-term millennial-scale variability during the late Glacial period, as evident from the *G. bulloides*, *G. glutinata* and *G. falconensis* records. Maximum abundances of *G. ruber* occur between 15 and 13 kyr BP, a period equivalent to the warm Bølling/Allerød (B/A) event, and in the early Holocene between 9 and 6 kyr BP (Fig. 3). A prominent decline in its abundance is noticed during the YD between 13 and 11 kyr BP and

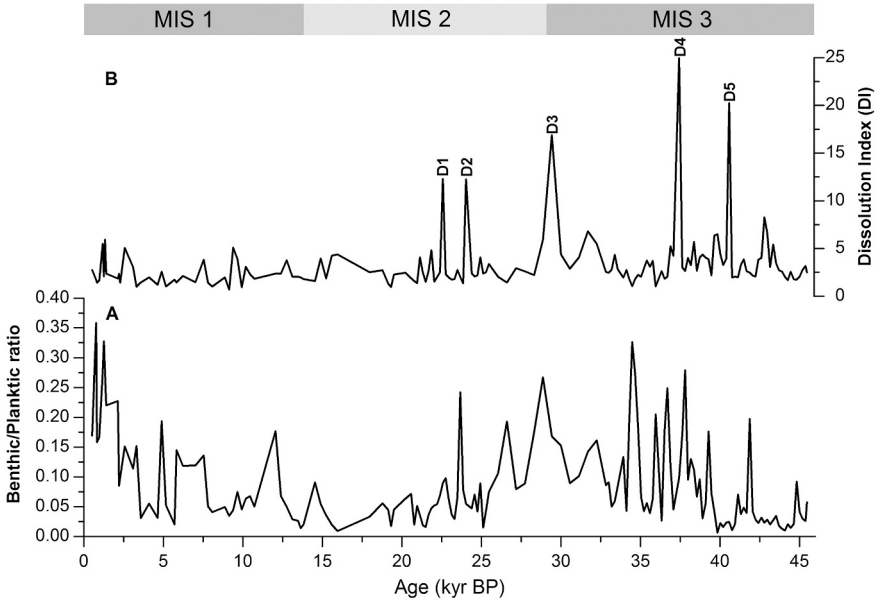


**Fig. 2.** (A) Records of Benthic/Planktic foraminiferal abundance ratio (no. of benthic foraminifera/total no. of benthic+planktic foraminifera in 1 g dry sediment >125 μm). (B) Dissolution Index (DI) (no. of dissolution resistant/dissolution susceptible planktic foraminifera in 1 g dry sediment >125 μm). Dissolution resistant species: *N. dutertrei*, *G. tumida*, *G. menardii*, *P. obliquiloculata*; Dissolution susceptible species: *G. bulloides*, *G. glutinata*, *G. ruber*, *G. rubescens*, *G. aquilateralis*, *T. sacculifer* plexus. D1-D5 are the plausible dissolution events. Horizontal grey bar indicates the Marine Isotope Stages, MIS 1–3.

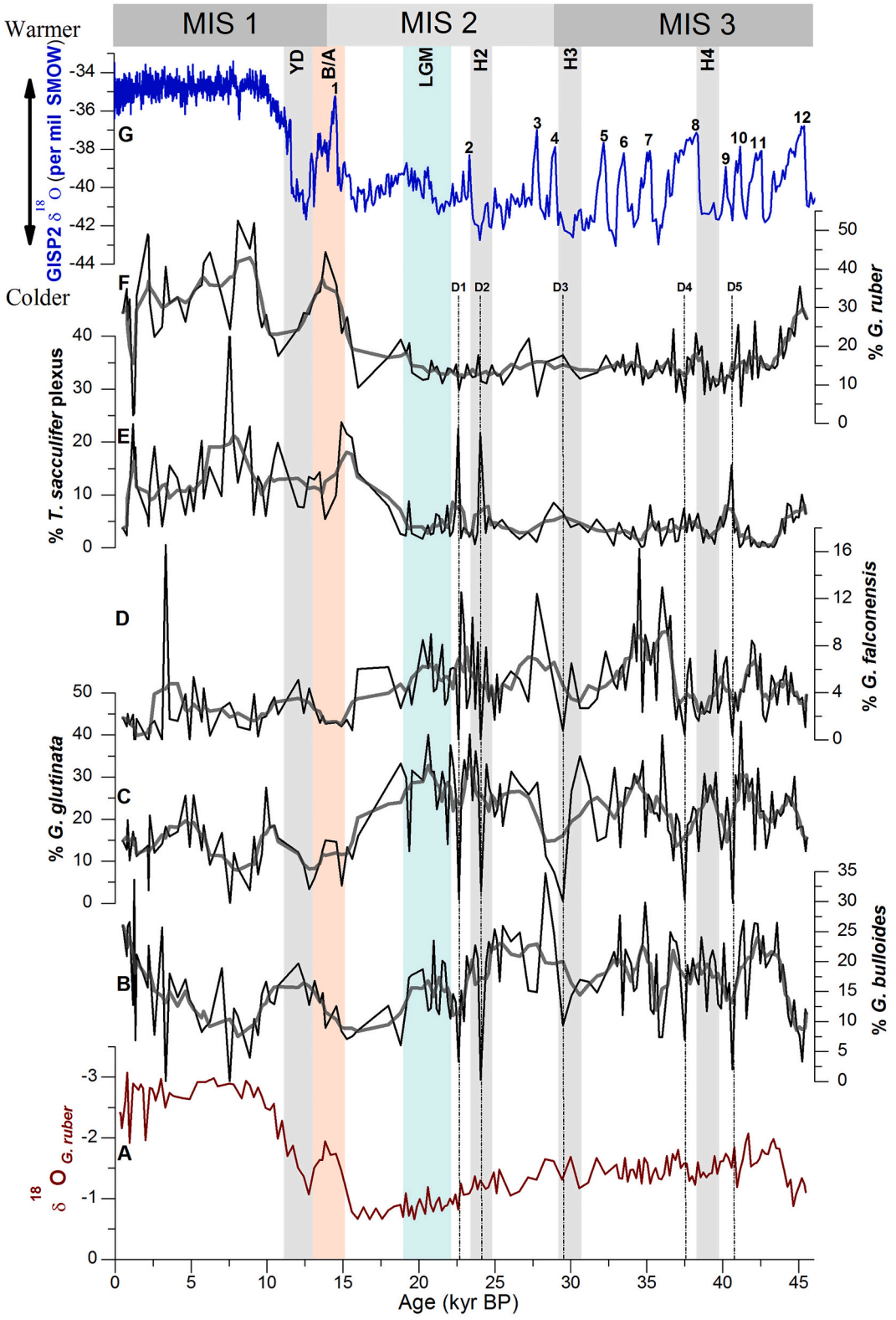


**Fig. 3.** Comparison of relative abundances of mixed-layer planktic foraminiferal species in core SK 218/1 (this study) with $\delta^{18}O$ record of a surface dwelling planktic foraminifera in core SK 218/1 (record of the last 32 kyr BP is from Naidu and Govil (2010)) and GISP2 ice core record (Stuiver and Grootes, 2000): (A) $\delta^{18}O$ of *G. ruber*, (B) % *G. bulloides*, (C) % *G. glutinata*, (D) % *G. falconensis*, (E) % *T. sacculifer* plexus, (F) % *G. ruber* and (G) GISP2 ice core $\delta^{18}O$ record. Bold lines show 5 point running average. The numbers 1–12 in the GISP2 $\delta^{18}O$ record denote the D/O interstadials. The grey shaded vertical bars represent Younger Dryas (YD) and Heinrich events (H2-H4). Pink and blue shaded vertical bars represent the Bølling-Allerød (B/A) and Last Glacial Maximum (LGM) periods respectively. Horizontal grey bar indicates the Marine Isotope Stages, MIS 1–3. D1-D5 (dotted lines) are inferred dissolution events. (For interpretation of the references to colour in this figure legend, the reader is referred to the web version of this article.)

5 and 3 kyr BP. After showing a trend of significant increase from 3 kyr BP, *G. ruber* abundance declined since 1.5 kyr BP (Fig. 3).

## 5. Discussion

### 5.1. Planktic foraminiferal assemblage response to the seasonal changes in surface hydrography

Plankton net and sediment trap studies in the Northern Indian Ocean revealed large variations in planktic foraminiferal shell fluxes and species composition in response to the seasonal monsoon circulations (e.g., Kroon, 1991; Curry et al., 1992; Conan and Brummer, 2000; Guptha et al., 1997). The sediment trap experiment conducted in the BoB has shown bimodal patterns in biogenic (including planktic foraminifera) fluxes related to the SW and NE monsoons (Guptha et al., 1997; Vidya and Prasanna Kumar, 2013). The seasonal pattern of biogenic flux in the BoB is attributed to changes in the upper water column structure and nutrient state of the mixed-layer due to the seasonal monsoon induced fluvial influx, surface water stratification and wind driven upwelling and/or mixing. High fluvial influx to the BoB associated with SW monsoons restricts upwelling and wind-driven upward transport of nutrients to the euphotic zone leading to low plankton production (Unger et al., 2003; Prasanna Kumar et al., 2010). Besides, the wind-induced mixing drives the winter phytoplankton bloom in the western BoB south of 17° N and west of 90° E (Martin and Shaji, 2015). Therefore, the fluvial input and wind forcing together modulate the year-round surface conditions and biogenic shell fluxes in the BoB (Unger et al., 2003).

Planktic foraminifera living in the mixed-layer strongly respond to changes in surface hydrographic and nutrient conditions. The *G. ruber* and *T. sacculifer* plexus represents tropical warm water species; which are known to have adapted to low-nutrient oligotrophic environments (Bé and Hamlin, 1967; Bé and Hutson, 1977; Bé and Tolderlund, 1971; Hemleben et al., 1989; Spindler et al., 1984; Guptha et al., 1997). *G. bulloides, G. glutinata* and *G. falconensis* are eutrophic species, which thrive in nutrient-rich, highly mixed surface waters associated with tropical upwelling and/or vertical mixing (Bé and Tolderlund, 1971; Cullen and Prell, 1984; Kroon, 1991; Singh et al., 2011, 2018). The sediment trap flux record from the BoB exhibits elevated *G. bulloides* fluxes during the SW monsoon season in the western BoB and during the NE monsoon season in the northern BoB (Guptha et al., 1997; Stoll et al., 2007). Previous studies from other areas have also shown high abundances of *G. bulloides* during both the SW and NE monsoon seasons (e.g., Sautter and Thunell, 1991). Although the annual flux of *G. glutinata* in the northern BoB is higher than in the western BoB, it shows elevated flux during the NE monsoon season (Guptha et al., 1997). Unlike *G. bulloides*, this species feeds on diatoms and its abundant occurrence in the northeastern Arabian Sea waters during the NE monsoon is linked with the winter diatom bloom (Spindler et al., 1984; Schulz et al., 2002). Hence, the two distinct groups of species: mixed-layer eutrophic species (MLES) and mixed-layer oligotrophic species (MLOS) are related to the different modes of surface ocean conditions and nutrient state of the mixed-layer (e.g., Singh et al., 2018). High abundance of MLOS (*G. ruber, T. sacculifer* plexus) is indicative of strongly stratified and nutrient-poor (oligotrophic) mixed-layer water and low biological productivity. Whereas, increased abundances of MLES (*G. bulloides, G. glutinata, G. falconensis*) is related to highly mixed nutrient-rich (eutrophic) waters in the mixed-layer and high biological productivity. Additionally, the relative abundance ratio of *G. bulloides* and *G. ruber* should also reflect surface ocean conditions, as the former represents well mixed eutrophic waters and the latter stratified oligotrophic waters (Conan and Brummer, 2000; Singh et al., 2006, 2011; Stoll et al., 2007). Sediment trap studies in the Arabian Sea have reported moderate to high values of *G. bulloides/G. ruber* during wind induced mixing and upwelling conditions and minimum values during highly stratified non-upwelling conditions (Conan and Brummer, 2000). The response of this proxy to seasonal changes in the upper water column of the BoB is also comparable with the Arabian Sea (Stoll et al., 2007). Therefore, the *G. bulloides/G. ruber* ratio is a potential proxy to record changes in the mixed-layer environment (surface stratification and trophic conditions) [Conan and Brummer, 2000; Stoll et al., 2007; Singh et al., 2006, 2011]. High values represent highly mixed eutrophic waters, whereas low values indicate stratified oligotrophic waters within the mixed-layer.

### 5.2. Millennial–scale productivity variations in relation to seasonal monsoon-driven hydrographic changes during the late Glacial period (45–19 kyr BP)

Our faunal proxy records (% individual species, MLES vs. MLOS abundances and *G. bulloides/G. ruber* ratio) reflect pronounced changes during the late Glacial, the deglacial and Holocene periods on a millennial time scale (Figs. 3, 4). Overall high abundances of MLES and corresponding very low abundances of MLOS (<15%) between 44 and 19 kyr BP during marine isotope stages (MIS) 2–3 (Fig. 4) suggest that the late Glacial productivity was relatively higher as compared to the deglacial and Holocene periods. Within this time interval, however, the abundance record of MLES exhibits significant variations on a millennial-scale (Figs. 3, 4). The prominent peaks of MLES abundances (> 50%) occurring during 43–41, 39.5–38.5, 35–34, 31.5–30, 28.5–28, 27–25, 24–23 and 22–19 kyr BP might be related to the nutrient-rich, eutrophic conditions in highly mixed surface water. The high values of the *G. bulloides/G. ruber* ratio during these periods further support the notion of less stratified surface water and high productivity conditions attributed to the vertical advection of nutrient-rich subsurface water into the euphotic zone leading to the increased phytoplankton growth. The productivity maxima during 39.5–38.5, 31.5–30 and 24–23 kyr BP apparently correspond to the North Atlantic cold Heinrich (H) events 4, 3 and 2 respectively. However, a part of the record of surface hydrographic conditions during H2 and H3 events is obliterated due to carbonate dissolution (D2 and D3) (Fig. 4). Our proxy records clearly suggest that the productivity increase during the H4 event was more pronounced compared to H2 and H3. Modelling experiments have demonstrated a close relationship between the North Atlantic SST and the Indian monsoon intensity (Goswami et al., 2006; Feng and Hu, 2008). A warm (cold) phase of the North Atlantic is associated with strong (weak) SW Indian monsoon (Zhang and Delworth, 2006; Lu et al., 2006). Previous paleoceanographic studies in the Arabian Sea and Bay of Bengal have also shown a weaker SW monsoon and enhanced NE monsoon wind circulation during cold Heinrich events and stadials (Colin et al., 1998; Reichart et al., 1998, 2004; Schulz et al., 1998; Kudrass et al., 2001; Schulte and Müller, 2001; Klöcker and Henrich, 2006; Marzin et al., 2013; Deplazes et al., 2014; Ali et al., 2015). Hence, the productivity maxima during Heinrich events are most likely related to the intensification of NE monsoonal winds driving the injection of nutrients from deep waters into the mixed-layer. The positive excursion in $\delta^{18}O_{sw}$ values during the H2 event suggests low monsoon freshwater flux at the core site (Govil and Naidu, 2011) (Fig. 4). The reduced freshwater flux due to a weakened SW monsoon resulted in a less stable upper water column, which favoured enhancement of nutrient entrainment by wind driven processes and vertical mixing during the NE monsoon. A moderate decline in productivity from 23 to 22 kyr BP as reflected by decreased abundances of MLES and low values of *G. bulloides/G. ruber* ratio is probably associated to the stratified surface water conditions due to increased freshwater influx at the core site. Surface ocean freshening between 23 and 22 kyr BP is evident from the $\delta^{18}O_{sw}$ record (Govil and Naidu, 2011) (Fig. 4). Ota et al. (2019) suggested a significant decrease in SW monsoon precipitation in the northeastern and eastern part of the Indian peninsula and related freshwater outflow to BoB during MIS 2. Therefore, low $\delta^{18}O_{sw}$ values during 23–22 kyr BP are likely related to the regional freshening probably due to the enhanced NE monsoon precipitation over south-eastern India leading to high freshwater influx at the core location (Govil and Naidu, 2011). The surface ocean stratification might have impeded the

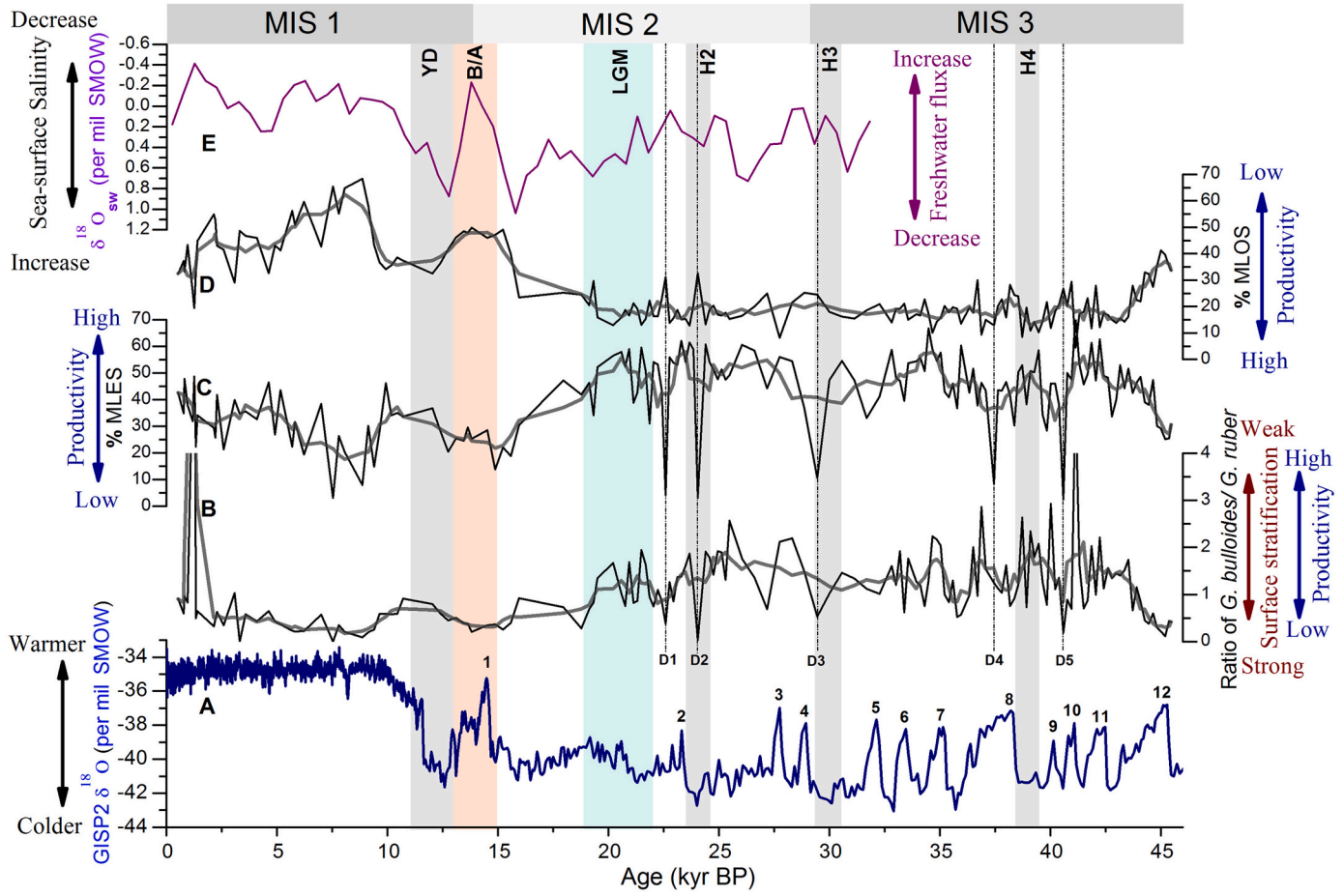


**Fig. 4.** Records of faunal proxies for surface water stratification and productivity (this study) are compared with sea-surface salinity record of core SK218/1 (Govil and Naidu, 2011) and GISP2 ice core $\delta^{18}O$ record (Stuiver and Grootes, 2000): (A) GISP2 ice core $\delta^{18}O$; (B) ratio of *G. bulloides* and *G. ruber*; (C) % MLES (Mixed-layer eutrophic species; *G. bulloides*, *G. glutinata* and *G. falconensis*); (D) % MLOS (Mixed-layer oligotrophic species; *G. ruber* and *T. sacculifer* plexus) and (E) $\delta^{18}O_{sw}$ (‰ SMOW) of core SK218/1. Bold lines show 5 point running average. The numbers 1–12 in the GISP2 $\delta^{18}O$ record denote the D/O interstadials. The grey shaded vertical bars represent Younger Dryas (YD) and Heinrich events (H2-H4). Pink and blue shaded vertical bars represent the Bølling-Allerød (B/A) and Last Glacial Maximum (LGM) periods respectively. Horizontal grey bar indicates the Marine Isotope Stages (MIS) 1–3. D1-D5 (dotted lines) are inferred dissolution events. (For interpretation of the references to colour in this figure legend, the reader is referred to the web version of this article.)

wind driven mixing process that can inject nutrients to the euphotic zone, as a consequence the productivity declined during this time interval. A conspicuous increase in SSS during the phases of productivity maxima between 27 and 25 kyr BP and during the Last Glacial Maximum (LGM) between 22 and 19 kyr BP (Fig. 4) implies that the freshwater flux was considerably reduced, which can be explained by a significant reduction in SW monsoon precipitation and river discharge around the western BoB. Relatively high values of *G. bulloides*/*G. ruber* ratios during these periods suggest a weakly stratified upper water column and enhanced mixing driven by the intensified NE monsoon wind circulation.

A striking difference in the abundance patterns of the two eutrophic species (*G. bulloides* and *G. glutinata*) during these two intervals of productivity maxima (27–25 kyr BP and 22–19 kyr BP) (Fig. 3) points towards a change in the strength of the vertical mixing process. *G. bulloides* thrives in deeply mixed nutrient-rich cold waters associated with vertical advection of deep waters to the surface, whereas *G. glutinata* being a nutrient loving cosmopolitan species can flourish even in shallow mixed eutrophic waters. The predominance of *G. glutinata* over *G. bulloides* during LGM in contrast to 27–25 kyr BP when the abundance of both species was equally enhanced, suggests a more pronounced and deep mixing in the later period. Earlier studies have suggested a weakened SW monsoon during the LGM because of a permanent Tibetan ice cover (Prell et al., 1980; Van Campo et al., 1982; Duplessy, 1982; Zhang and Delworth, 2005). Nevertheless, it is to be noted that the LGM was not the coldest glacial period in the mid-latitude North Atlantic (Duplessy et al., 1991; Marzin et al., 2013), hence the SW monsoon may have not been at its weakest mode during this time. We assume that although the NE monsoon circulation strengthened during the LGM, it was not probably that strong because SST in tropical regions was 2–3 °C lower contributing to a low land-sea pressure gradient (Kienast et al., 2001; Rosenthal et al., 2003). We, therefore suggest that the productivity pattern in MIS 2 at the core location is strongly modulated by the magnitude of variations in the NE monsoon wind intensity and regional precipitation and continental runoff.

Our foraminiferal proxy records (MLES abundance and *G. bulloides*/*G. ruber* ratio) show high frequency variations during MIS 3 between 45 and 29 kyr BP (Fig. 4). The proxy records demonstrate alternating episodes of productivity maxima and minima in concert with the Northern Hemisphere climate events (D—O cycles and Heinrich events). The timing and sequence of productivity minima apparently correspond to the D—O warm interstadials and the maxima to the cold stadials and Heinrich events (H3 and H4) (Fig. 4). On a glacial/interglacial timescale, the intensity of the SW monsoon and associated precipitation during MIS 3 was relatively stronger compared to MIS 2 (Ota et al., 2019). However, the proxy records from the Arabian Sea on a millennial-scale (Reichart et al., 1998, 2004; Schulz et al., 1998; Singh et al., 2011; Deplazes et al., 2014) and BoB (Kudrass et al., 2001; Ahmad

et al., 2005; Rashid et al., 2011; Ali et al., 2015; Lauterbach et al., 2020; Liu et al., 2021) provided strong evidence for a weaker SW monsoon during the cold stadials (cold phases of the D—O events) and stronger monsoon during the interstadials (warm phases of the D—O events). Earlier studies also suggested the intensification of NE monsoon circulation during the cold stadials (Reichart et al., 1998, 2004; Klöcker and Henrich, 2006). Thus, the high productivity events during the cold stadials are most likely linked with the intensified NE monsoonal winds induced mixing and the injection of nutrient-rich subsurface waters into the euphotic zone. Alternatively, the low productivity during the warm interstadials is related to the prevalence of strongly stratified surface ocean conditions coupled with subdued winter mixing. An intensified SW monsoon during interstadials would result in a high freshwater influx to the BoB and that would cause a strong surface ocean stratification and oligotrophic conditions in the mixed-layer. Significant upwelling during the SW monsoon is unlikely to occur in the BoB (Gebregiorgis et al., 2016), which could enhance the vertical advection of nutrient-rich deep waters to the surface. However, some increase in productivity related to local hydrographic processes during warm interstadials is not completely ruled out. Nevertheless, it is clearly evident from our faunal records that year-round productivity during stadials is much higher than during interstadials. Our results from the BoB are in contrast to the northern and western Arabian Sea, where the productivity has been reported to be high during the interstadials driven by stronger SW monsoon induced upwelling (Reichart et al., 1998; Schulz et al., 1998; Altabet et al., 2002; Deplazes et al., 2014). We, therefore, conclude that the D—O variability in the surface hydrography and productivity in the western BoB is primarily governed by changes in the intensity of SW monsoon related precipitation and continental runoff and the NE monsoon wind circulation.

### 5.3. Enhanced influence of SW monsoon on productivity pattern since the last deglaciation (19 kyr BP to present)

The planktic foraminiferal assemblage record shows a major change between 19 and 15 kyr BP indicating a prominent shift from the high productive environment of the LGM to relatively low productivity conditions (Fig. 4). A gradual reduction in the abundances of MLES between 19 and 17 kyr BP, followed by a rapid decline in their abundances during 16–15 kyr BP suggests a two-step change in surface hydrography and productivity in response to the variation in seasonal monsoon circulation during the early deglacial period (Figs. 3, 4). The abundance variation pattern of MLES which is opposite to that of MLOS, follows the pattern of SSS variations (Govil and Naidu, 2011) (Fig. 4). Earlier studies have shown that the SW monsoon was weaker (Sirocko et al., 1993; Rashid et al., 2011), although the NE monsoon intensified during the early deglacial period between 19 and 17 kyr BP (Tiwari et al., 2005). A reduction in SSS during this period (Govil and Naidu, 2011) attributed to the increased precipitation and river runoff from peninsular India in the NE monsoon season (Tiwari et al., 2005) would have led to a salinity stratification in the mixed-layer. It is likely that the north-easterly winds were strong enough to promote shallow vertical mixing and entrainment of nutrient-rich subsurface waters to the euphotic zone leading to a moderate increase in productivity. It is interesting to note that the abundance of *G. glutinata*, a species associated to the diatom bloom remained high, however *G. bulloides* abundance decreased significantly between 19 and 17 kyr BP, which supports our conclusion of a moderate increase in productivity during this period due to shallow winter mixing. A significant reduction of all eutrophic species and a corresponding increase of oligotrophic species during 16–15 kyr BP are indicative of strongly stratified, nutrient-poor mixed-layer waters and low productivity conditions (Figs. 3, 4). It is convincingly apparent that there has been a major reorganization of seasonal monsoon wind circulation after 16 kyr BP, when the SW monsoon intensified and concomitantly the NE monsoon weakened. A rapid and conspicuous reduction in SSS coupled with surface warming between 16 and 13 kyr BP (Govil and Naidu, 2011) point towards the strong stratification of the surface ocean, reduced vertical mixing and low productivity conditions during this period. This is in agreement with other SSS and SST records from the BoB (Kudrass et al., 2001) and Arabian Sea (Anand et al., 2008).

High abundances of MLOS and corresponding low MLES abundances and very low values of *G. bulloides/G. ruber* ratio between 15 and 13 kyr BP (Fig. 4), a period broadly equivalent to the warm B/A event, indicate low productivity and strongly stratified surface waters, which can be attributed to the intensified SW monsoon precipitation and increased runoff from the continent. Strong salinity stratification due to large freshwater influx inhibited the wind-driven upward transport of nutrients to the euphotic zone resulting in low productivity. A conspicuous surface water freshening during this period is evident from the $\delta^{18}O_{sw}$ record (Govil and Naidu, 2011) (Fig. 4). The productivity increased between 13 and 11 kyr BP as evidenced by high abundances of MLES and concomitant decline of MLOS. A moderate increase in *G. bulloides/G. ruber* values points towards a less stratified surface water conditions. This time interval apparently corresponds to the northern Hemisphere cold YD event, a period when the SW monsoon was relatively weak as reflected in SSS records from the Arabian Sea (Anand et al., 2008) and BoB (Kudrass et al., 2001; Rashid et al., 2011; Govil and Naidu, 2011; Liu et al., 2021) (Fig. 5). Low amount of freshwater influx due to a weakened SW monsoon might have resulted in less stratified surface ocean conditions, which favoured the transport of nutrients from subsurface waters to the euphotic zone driven by relatively stronger NE monsoon winds induced vertical mixing.

The faunal proxies combined with the $\delta^{18}O_{sw}$ record (Govil and Naidu, 2011) indicate a rapid shift in surface ocean conditions from less stratified, nutrient-rich surface waters to the strongly stratified, nutrient-poor waters between 11 and 9 kyr BP, probably triggered by a major change in SW monsoon intensity (Fig. 4). High abundances of MLOS during the Holocene between 9 and 1.5 kyr BP suggest overall low productivity conditions associated with stratified, nutrient-poor waters in the mixed-layer. This observation agrees with the overall low *G. bulloides/G. ruber* ratio. Our faunal results are consistent with the SSS record of the core (Govil and Naidu, 2011) indicating surface freshening (Fig. 4). The $\delta^{18}O_{sw}$ is strongly controlled by SW monsoon precipitation and associated freshwater discharge to the BoB during the Holocene (Rashid et al., 2011; Liu et al., 2021). During this period, however, the faunal record further indicates that the productivity was lowest between 9 and 6 kyr BP and then increased gradually between 5 and 3 kyr BP as evidenced by a moderate increase in MLES. This implies that the SW monsoon was strongest during 9–6 kyr BP favouring a high freshwater flux and intensification of surface ocean stratification at the core location, but the monsoon intensity and associated fluvial discharge gradually declined from 5 to 3 kyr BP. The increased $\delta^{18}O_{sw}$ values between 5 and 3 kyr BP further support the notion of a weakened SW monsoon (Rashid et al., 2011; Govil and Naidu, 2011). The productivity values during this period (5–3 kyr BP) increased moderately, when surface water stratification weakened due to reduced SW monsoon precipitation. The faunal and $\delta^{18}O_{sw}$ records further reveal a reduction in productivity associated with the moderately stratified surface ocean conditions due to a relative increase in SW monsoon precipitation between 3 and 1.5 kyr BP (Fig. 4).

### 5.4. Regional response of the SW monsoon

Our foraminiferal proxy records from the western BoB showing millennial-scale variability of surface hydrography and productivity are profoundly influenced by the changes in the continental runoff related primarily to the SW monsoon intensity. The overall pattern of the proxy records agrees well with other monsoon proxy records from the BoB (Kudrass et al., 2001; Rashid et al., 2011; Liu et al., 2021), Andaman Sea (Rashid et al., 2007; Gebregiorgis et al., 2016) and the Hulu Cave speleothem (Wang et al., 2001) (Fig. 5). The millennial-scale perturbations in surface ocean conditions in the BoB are in concordance with the D—O

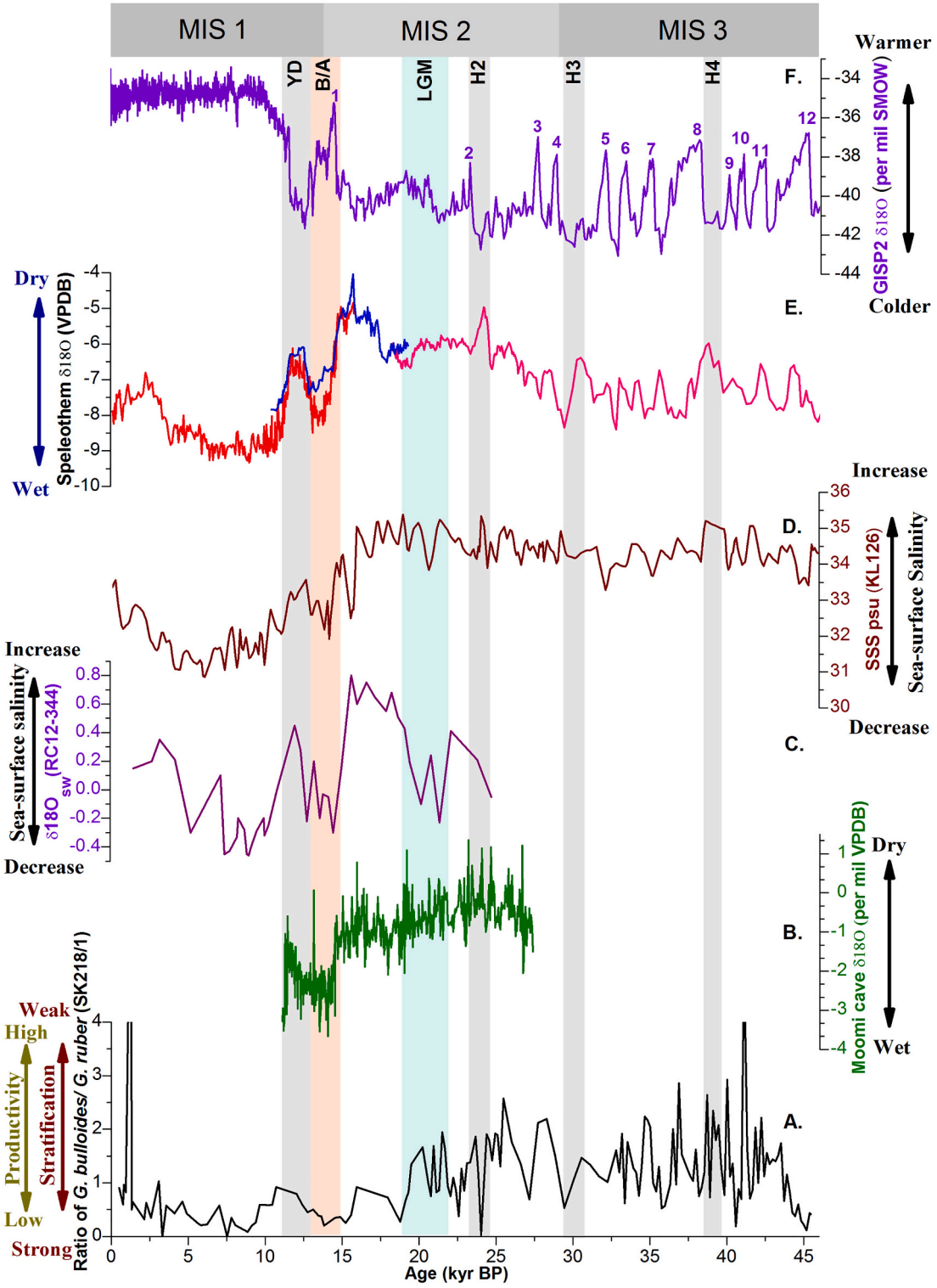


**Fig. 5.** Record of past changes in surface ocean conditions (stratification and productivity) in the western Bay of Bengal (SK218/1, this study) is compared with monsoon proxy records from other regions. (A) Ratio of *G. bulloides* and *G. ruber* (SK 218/1; this study); (B) $\delta^{18}O$ of stalagmite from Moomi Cave (Socotra Island; Shakun et al., 2007) (C) $\delta^{18}O_{sw}$ record of core RC 12–344 (Andaman Sea; Rashid et al., 2007); (D) Sea-surface salinity record of SO93-KL 126 (northern BoB; Kudrass et al., 2001); (E) Oxygen isotopic data of stalagmites from Dongge (red), Hulu (PD) (blue) and Hulu (MSD) (pink) caves (China; Wang et al., 2001; Yuan et al., 2004); (F) GISP2 ice core $\delta^{18}O$ record (Stuiver and Grootes, 2000). The numbers 1–12 in the GISP2 $\delta^{18}O$ record denote the D/O interstadials. The grey shaded vertical bars represent Younger Dryas (YD) and Heinrich events (H2-H4). Pink and blue shaded vertical bars represent the Bølling-Allerød (B/A) and Last Glacial Maximum (LGM) periods respectively. Horizontal grey bar indicates the Marine Isotope Stages, MIS 1–3. (For interpretation of the references to colour in this figure legend, the reader is referred to the web version of this article.)

oscillations (warmer interstadials and colder stadials) as reflected in the GISP2 $\delta^{18}O$ record (Stuiver and Grootes, 2000) and the North Atlantic cold Heinrich events suggesting a teleconnection between both regions. Past changes in year-round productivity in the BoB are related to the relative strength of salinity stratification associated with the amount of freshwater influx during the SW monsoon and the intensity of NE monsoon winds induced mixing of the upper water column. The productivity minima during warm phases of the D—O events are attributed to the large freshwater influx and consequent salinity stratification during the intensified SW monsoon, which inhibits vertical advection of nutrient-rich deep waters to the surface by the weaker NE monsoon winds. Conversely, the weakened SW monsoon leading to a reduced freshwater influx and surface stratification together with the intensified NE monsoon wind-induced vertical mixing resulted in high productivity during cold phases of the D—O events and during the LGM. Further, a major reorganization of seasonal monsoon wind circulations during the last deglacial period is also reflected in the speleothem records from Timta Cave (Sinha et al., 2011) in northern India, Moomi Cave (Shakun et al., 2007) in Yemen, Hulu and Dongge Caves (Wang et al., 2001; Yuan et al., 2004) in China and other sediment records from the BoB (e.g., Rashid et al., 2011; Liu et al., 2021) and Andaman Sea (Rashid et al., 2007; Gebregiorgis et al., 2016) (Fig. 5). All these records indicate enhanced SW monsoon precipitation during the warm B/A event, when productivity in the western BoB declined due to the strong surface stratification caused by the increased freshwater influx, whereas reduced SW monsoon precipitation during the cold YD event resulted in productivity increase due to the enhanced NE monsoon-induced vertical mixing of less stratified surface waters. Our interpretations of strongest SW monsoon in the early Holocene (9–6 kyr BP) and its relative weakening after 5 kyr BP are also in concordance with the earlier studies from the BoB (e.g., Kudrass et al., 2001) and Andaman Sea (Rashid et al., 2007; Gebregiorgis et al., 2016) (Fig. 5).

## 6. Conclusions

Abundance records of mixed layer planktic foraminifera (eutrophic and oligotrophic species/group) reveal major fluctuations in surface hydrography (extent of salinity stratification, mixing and trophic state) and productivity in response to the changes in intensity of seasonal monsoon (SW vs NE) precipitation and wind strength. The proxy records show millennial-scale variability which broadly corresponds to the Northern Hemisphere D—O oscillations and Heinrich events. Faunal proxy records suggest an overall high productivity during the late Glacial period between 44 and 19 kyr BP compared to the deglacial and Holocene periods. Within the late Glacial period, the maximum productivity occurred during the cold phases of D—O cycles (stadials) and North Atlantic Heinrich events (H2-H4). These productivity maxima are attributed to the less stratified upper water column due to the reduced SW monsoon related freshwater influx and the intensified NE monsoon winds induced vertical advection of nutrient-rich subsurface waters to the euphotic zone promoting enhanced phytoplankton growth. Conversely, low productivity events seem to occur during warm phases of the D—O events (interstadials), when SW monsoon intensified leading to an increase in freshwater influx and surface stratification which inhibited the vertical transport of nutrients from deep waters to the surface by the weaker NE monsoon winds.

Productivity was conspicuously low between 15 and 13 kyr BP, a period broadly equivalent to the warm B/A, when the mixed-layer was strongly stratified due to enhanced SW monsoon precipitation and river discharge from the continent. Between 13 and 11 kyr BP, surface ocean stratification weakened and productivity increased because of a reduction in freshwater influx due to weaker SW monsoon coupled with enhanced NE monsoon wind induced mixing. The productivity was lowest between 9 and 6 kyr BP, which is attributed to the intensification of SW monsoon precipitation and fluvial discharge leading to the strongly stratified surface ocean and oligotrophic conditions in the mixed-layer. The faunal record further suggests that the SW monsoon intensity and freshwater influx gradually declined from 5 to 3 kyr BP.

## Declaration of Competing Interest

The authors declare that they have no conflict of interest.

## Acknowledgements

We thank two anonymous referees, Guest Editor Ann Holbourn and the Editors (Thomas Algeo and H. J. Falcon-Lang) for their constructive reviews that have helped to improve the manuscript. This research was supported by the ISRO-GBP sponsored project (P-32-14) and IoE Incentive Grant BHU to ADS and IoE Seed Grant BHU (Dev. Scheme No. 6031) to KV. We wish to thank the scientific party and crew of ORV *Sagar Kanya* for coring the samples in western BOB. PS acknowledges to the Climate Change Programme of DST (DST/CCP/CoE/80/2017-G) for Junior Research Fellowship, HS to UGC for Senior Research Fellowship (419/(CSIR-UGC NET JUNE 2018)), RKS to CSIR for Senior Research Fellowship and PRU to UGC for Dr. D.S. Kothari postdoctoral fellowship (ES/17-18-0055).

## Appendix A. Supplementary data

Supplementary data to this article can be found online at https://doi.org/10.1016/j.palaeo.2022.110844.

## References

Ahmad, S.M., Anil Babu, G., Padmakumari, V.M., Dayal, A.M., Sukhija, B.S., Nagabhushanam Sr., P., 2005. Nd isotopic evidence of terrigenous flux variations in the Bay of Bengal: Implications of monsoons during the last 34000 years. Geophys. Res. Lett. 32, L22711.

Ali, S., Hathorne, E.C., Frank, M., Gebregiorgis, D., Stattegger, K., Stumpf, R., Kutterolf, S., Johnson, J.E., Giosan, L., 2015. South Asian monsoon history over the past 60 kyr recorded by radiogenic isotopes and clay mineral assemblages in the Andaman Sea. Geochem. Geophys. Geosyst. 16 (2), 505–521.

Altabet, M.A., Higginson, M.J., Murray, D.W., 2002. The effect of millennial-scale changes in Arabian Sea denitrification on atmospheric CO2. Nature 415, 159–162.

Anand, P., Kroon, D., Singh, A.D., Ganeshram, R.S., Ganssen, G., 2008. Coupled sea surface temperature-seawater δ18O reconstructions in the Arabian Sea at the millennial scale for the last 35 ka. Paleoceanography 23, PA4207.

Balachandran, K.K., Laluraj, C.M., Jyothibabu, R., Madhu, N.V., Muraleedharan, K.R., Vijay, J.G., Maheswaran, P.A., Ashraff, T.T.M., Nair, K.K.C., Achuthankutty, C.T., 2008. Hydrography and biogeochemistry of the north western Bay of Bengal and the north eastern Arabian Sea during winter monsoon. J. Mar. Syst. 73, 76–86.

Banse, K., 1987. Seasonality of phytoplankton chlorophyll in the central and northern Arabian Sea. Deep-Sea Res. 34, 713–723.

Bé, A.W.H., Hamlin, W.H., 1967. Ecology of recent planktonic foraminifera, part 3-distribution in the North Atlantic during the summer of 1962. Micropaleontology 13, 87–106.

Bé, A.W.H., Hutson, W.H., 1977. Ecology of planktonic foraminifera and biogeographic patterns of life and fossil assemblages in the Indian Ocean. Micropaleontology 27, 369–414.

Bé, A.W.H., Tolderlund, D.S., 1971. Distribution and ecology of living planktonic foraminifera in surface waters of the Atlantic and Indian Oceans. In: Funnel, B.M., Riedel, W.R. (Eds.), The Micropaleontology of Oceans, pp. 105–149.

Berger, W.H., 1973. Deep-sea carbonates: Pleistocene dissolution cycles. J. Foraminifer. Res. 3, 187–195.

Clemens, S.C., Prell, W.L., Murray, D., Shimmield, G., Weedon, G., 1991. Forcing mechanisms of the Indian Ocean monsoon. Nature 353, 720–725.

Colin, C., Kissel, C., Blamart, D., Turpin, L., 1998. Magnetic properties of sediments in the Bay of Bengal and the Andaman Sea: impact of rapid North Atlantic Ocean climatic events on the strength of the Indian monsoon. Earth Planet. Sci. Lett. 160, 623–635.

Conan, S.M.H., Brummer, G.-J.A., 2000. Fluxes of planktonic Foraminifera in response to monsoonal upwelling on the Somalia Basin margin. Deep-Sea Res. II Top. Stud. Oceanogr. (47), 2207–2227.

Cullen, J.L., Prell, W.L., 1984. Planktonic foraminifera of the northern Indian Ocean: distribution and preservation in surface sediments. Mar. Micropaleontol. 9 (1), 1–52.

Curry, W.B., Ostermann, D., Guptha, M.V.S., Ittekkot, V., 1992. Foraminiferal production and monsoonal upwelling in the Arabian Sea: evidence from sediment traps. Geol. Soc. Lond. Spec. Publ. 64 https://doi.org/10.1144/GSL.SP.1992.064.01.06.

Da Silva, R., Mazumdar, A., Mapder, T., Peketi, A., Joshi, R.K., Shaji, A., Mahalakshmi, P., Sawant, B., Naik, B.G., Carvalho, M.A., Molletti, S.K., 2017. Salinity stratification controlled productivity variation over 300 ky in the Bay of Bengal. Sci. Rep. 7, 14439. https://doi.org/10.1038/s41598-017-14781-3.

Deplazes, G., Luckge, A., Stuut, J.-B.W., Patzold, J., Kuhlmann, H., Husson, D., Fant, M., Haug, G.H., 2014. Weakening and strengthening of the Indian monsoon during Heinrich events and Dansgaard-Oeschger oscillations. Paleoceanography 29, 99–114. https://doi.org/10.1002/2013PA002509.

Dimri, A.P., Yasunari, T., Kotlia, B.S., Mohanty, U.C., Sikka, D.R., 2016. Indian winter monsoon: present and past. Earth Sci. Rev. 163, 297–322. https://doi.org/10.1016/j.earscirev.2016.10.008.

Duplessy, J.C., 1982. Glacial to Interglacial contrast in the Northern Indian Ocean. Nature 295, 494–498.

Duplessy, J.C., Labeyrie, L., Juillet-Leclerc, A., Maitre, F., Duprat, J., Sarnthein, M., 1991. Surface salinity reconstruction of the North Atlantic Ocean during the last glacial maximum. Oceanol. Acta 14, 311–324.

Feng, S., Hu, Q., 2008. How the North Atlantic multi-decadal oscillation may have influenced the Indian summer monsoon during the past two millennia. Geophys. Res. Lett. 35, L01707. https://doi.org/10.1029/2007GL032484.

Gebregiorgis, D., Hathorne, E.C., Sijinkumar, A.V., Nagender Nath, B., Nürnberg, D., Frank, M., 2016. South Asian summer monsoon variability during the last ~54 kyrs inferred from surface water salinity and river runoff proxies. Quat. Sci. Rev. 138, 6–15. https://doi.org/10.1016/j.quascirev.2016.02.012.

Gomes, H.R., de Rada, S., Goes, J.I., Chai, F., 2016. Examining features of enhanced phytoplankton biomass in the Bay of Bengal using a coupled physical-biological model. J. Geophys. Res. 121, 5112–5133. https://doi.org/10.1002/2015JC011508.

Goswami, B.N., Madhusoodanan, M.S., Neema, C.P., Sengupta, D., 2006. A physical mechanism for the North Atlantic SST influence on the Indian summer monsoon. Geophys. Res. Lett. 33, L02706. https://doi.org/10.1029/2005GL024803.

Govil, P., Naidu, P.D., 2011. Variations of Indian monsoon precipitation during the last 32 kyr reflected in the surface hydrography of the Western Bay of Bengal. Quat. Sci. Rev. 30, 3871–3879.

Guptha, M.V.S., Curry, W.B., Ittekkot, V., Muralinath, A.S., 1997. Seasonal variation in the flux of planktic Foraminifera; sediment trap results from the Bay of Bengal, northern Indian Ocean. J. Foraminifer. Res. 27 (1), 5–19. https://doi.org/10.2113/gsjfr.27.1.5.

Hastenrath, S., Greischar, L., 1989. Upper-ocean structure. In: Climatic Atlas of the Indian Ocean, vol. 3. University of Wisconsin Press, p. 273.

Hemleben, C., Spindler, M., Anderson, O.R., 1989. Modern Planktonic Foraminifera. Springer, New York, p. 363.

Ittekkot, V., Nair, R.R., Honjo, S., Ramaswamy, V., Bartsch, M., Manganini, S., Desai, B. N., 1991. Enhanced particle fluxes in Bay of Bengal induced by injection of freshwater. Nature 351, 385–387.

Ivanova, E.V., Schiebel, R., Singh, A.D., Schmiedl, G., Niebler, H.-S., Hemleben, C., 2003. Primary production in the Arabian Sea during the last 135,000 years. Palaeogeogr. Palaeoclimatol. Palaeoecol. 197 (1–2), 61–82.

Joussain, R., Colin, C., Liu, Z., Meynadier, L., Fournier, L., Fauquembergue, K., Zaragosi, S., Schmidt, F., Rojas, V., Bassinot, F., 2016. Climatic control of sediment transport from the Himalayas to the proximal NE Bengal Fan during the last glacial-interglacial cycle. Quat. Sci. Rev. 148, 1–16.

Kennett, J.P., Srinivasan, M.S., 1983. Neogene Planktonic Foraminifera: A Phylogenetic Atlas. Hutchinson Ross Publishing Company, Stroudsburg, pp. 1–265.

Kienast, M., Steinke, S., Stattegger, K., Calvert, S.E., 2001. Synchronous tropical South China Sea SST change and Greenland warming during deglaciation. Science 291 (5511), 2132–2134. https://doi.org/10.1126/science.1057131.

Klöcker, R., Henrich, R., 2006. Recent and late Quaternary pteropod preservation on the Pakistan shelf and continental slope. Mar. Geol. 231 (1–4), 103–111.

Kroon, D., 1991. Distribution of extant planktic foraminiferal assemblages in Red Sea and northern Indian Ocean surface waters. Rev. Esp. Micropaleontol. 13 (1), 37–74.

Kroon, D., Beets, K., Mowbray, S., Shimmield, G., Steens, T., 1990. Changes in northern Indian Ocean monsoonal wind activity during the last 500 ka. Mem. Della Soc. Geol. Ital. 44, 189–207.

Kudrass, H.R., Hofmann, A., Doose, H., Emeis, K., Erlenkeuser, H., 2001. Modulation and amplification of climatic changes in the Northern Hemisphere by the Indian summer monsoon during the past 80 k.y. Geology 29, 63–66.

Kumar, S., Ramesh, R., Sardesai, S., Sheshshayee, M.S., 2004. High new production in the Bay of Bengal: possible causes and implications. Geophys. Res. Lett. 31, L18304. https://doi.org/10.1029/2004GL021005.

Lauterbach, S., Andersen, N., Wang, Y.V., Blanz, T., Larsen, T., Schneider, R.R., 2020. A ~130 kyr record of surface water temperature and δ18O from the northern Bay of Bengal: investigating the linkage between Heinrich events and weak monsoon intervals in Asia. Paleoceanogr. Paleoclimatol. 35 (2) https://doi.org/10.1029/2019PA003646.

Li, J., Liu, S., Shi, X., Zhang, H., Fang, X., Cao, P., Yang, G., Xue, X., Khokiattiwong, S., Kornkanitnan, N., 2019. Sedimentary responses to the sea level and Indian summer monsoon changes in the central Bay of Bengal since 40 ka. Mar. Geol. 415, 105947.

Liu, S., Ye, W., Cao, P., Zhang, H., Chen, M.-T., Li, X., Li, J., Pan, H.-J., Khokiattiwong, S., Kornkanitnan, N., Shi, X., 2021. Paleoclimatic responses in the tropical Indian Ocean to regional monsoon and global climate change over the last 42 kyr. Mar. Geol. 438, 106542.

Lu, R., Dong, B., Ding, H., 2006. Impact of the Atlantic Multidecadal Oscillation on the Asian summer monsoon. Geophys. Res. Lett. 33, L24701.

Lübbers, J., Kuhnt, W., Holbourn, A.E., Bolton, C.T., Gray, E., Usui, Y., Kochhann, K.G.D., Beil, S., Andersen, N., 2019. The middle to late miocene "Carbonate Crash" in the Equatorial Indian Ocean. Paleoceanogr. Paleoclimatol. 34 (5), 813–832.

Madhupratap, M., Kumar, S.P., Bhattathiri, P.M.A., Kumar, M.D., Raghukumar, S., Nair, K.K.C., Ramaiah, N., 1996. Mechanism of the biological response to winter cooling in the northeastern Arabian Sea. Nature 384, 549–552.

Martin, M.V., Shaji, C., 2015. On the eastward shift of winter surface chlorophyll-a bloom peak in the Bay of Bengal. J. Geophys. Res. Oceans 120 (3), 2193–2211. https://doi.org/10.1002/2014jc010162.

Martinson, D.G., Pisias, N.G., Hays, J.D., Imbrie, J., Moore Jr., T.C., Shackleton, N.J., 1987. Age dating and the orbital theory of the ice ages: Development of a high-resolution 0 to 300,000-year chronostratigraphy. Quat. Res. 27 (1), 1–29.

Marzin, C., Kallel, N., Kageyama, M., Duplessy, J.C., Braconnot, P., 2013. Glacial fluctuations of the Indian monsoon and their relationship with North Atlantic climate: new data and modelling experiments. Clim. Past 9 (5), 2135–2151.

McCreary, J.P., Kundu, P.K., Molinari, R.L., 1993. A numerical investigation of dynamics, thermodynamics and mixed-layer processes in the Indian Ocean. Prog. Oceanogr. 31 (3), 181–244.

Murty, V.S.N., Sarma, Y.V.B., Rao, D.P., Murty, C.S., 1992. Water characteristics, mixing and circulation in the Bay of Bengal during southwest monsoon. J. Mar. Res. 50 (2), 207–228.

Naidu, P.D., Govil, P., 2010. New evidence on the sequence of deglacial warming in the tropical Indian Ocean. J. Quat. Sci. 25, 1138–1143. https://doi.org/10.1002/jqs.1392.

Naidu, P.D., Malmgren, B.A., 1996. A high resolution record of late Quaternary upwelling along the Oman margin, Arabian Sea based on planktonic foraminifera. Paleoceanogr. Paleoclimatol. 11 (1), 129–140.

Narvekar, J., Prasanna Kumar, S., 2006. Seasonal variability of the mixed layer in the central Bay of Bengal and associated changes in nutrients and chlorophyll. Deep-Sea Res. I Oceanogr. Res. Pap. 53 (5), 820–835.

Narvekar, J., Prasanna Kumar, S., 2014. Mixed layer variability and chlorophyll *a* biomass in the Bay of Bengal. Biogeosciences 11, 3819–3843. https://doi.org/10.5194/bg- 11-3819-2014.

Nilsson-Kerr, K., Anand, P., Sexton, P.F., Leng, M.J., Misra, S., Clemens, S.C., Hammond, S.J., 2019. Role of Asian summer monsoon subsystems in the inter-hemispheric progression of deglaciation. Nat. Geosci. 12, 290–295.

Ota, Y., Kuroda, J., Yamaguchi, A., Suzuki, A., Araoka, D., Ishimura, T., Kawahata, H., 2019. Monsoon-influenced variations in plankton community structure and upper-water column stratification in the western Bay of Bengal during the past 80 ky. Palaeogeogr. Palaeoclimatol. Palaeoecol. 521, 138–150.

Pattan, J.N., Mir, I.A., Parthiban, G., Karapurkar, S.G., Matta, V.M., Naidu, P.D., Naqvi, S.W.A., 2013. Coupling between suboxic condition in sediments of the western Bay of Bengal and southwest monsoon intensification: a geochemical study. Chem. Geol. 343, 55–66.

Peeters, F.J.C., Brummer, G.-J.A., 2002. The seasonal and vertical distribution of living planktic foraminifera in the NW Arabian Sea. In: Clift, P., Kroon, D., Gaedicke, C., Craig, J. (Eds.), Tectonic and Climatic Evolution of the Arabian Sea Region, Geological Society Special Publication, vol. 195, pp. 463–497.

Poole, C.R., Wade, B.S., 2019. Systematic taxonomy of the *Trilobatus sacculifer* plexus and descendant *Globigerinoidesella fistulosa* (planktonic foraminifera). J. Syst. Palaeontol. https://doi.org/10.1080/14772019.2019.1578831.

Prajith, A., Tyagi, A., Kurian, P.J., 2018. Changing sediment sources in the Bay of Bengal: evidence of summer monsoon intensification and ice-melt over Himalaya during the late Quaternary. Palaeogeogr. Palaeoclimatol. Palaeoecol. 511, 309–318. https://doi.org/10.1016/j.palaeo.2018.08.016.

Prasanna Kumar, S., Muraleedharan, P.M., Prasad, T.G., Gauns, M., Ramaiah, N., de Souza, S.N., Sardesai, S., Madhupratap, M., 2002. Why is the Bay of Bengal less productive during summer monsoon compared to the Arabian Sea? Geophys. Res. Lett. 29 (24), 22–35.

Prasanna Kumar, S., Nuncio, M., Ramaiah, N., Sardesai, S., Narvekar, J., Fernandes, V., Paul, J.T., 2007. Eddy-mediated biological productivity in the Bay of Bengal during fall and spring intermonsoons. Deep-Sea Res. I Oceanogr. Res. Pap. 54, 1619–1640.

Prasanna Kumar, S., Nuncio, M., Narvekar, J., Ramaiah, N., Sardesai, S., Gauns, M., Fernandes, V., Paul, J.T., Jyothibabu, R., Jayaraj, K.A., 2010. Seasonal cycle of physical forcing and biological response in the Bay of Bengal. Indian J. Mar. Sci. 39 (3), 388–405.

Prell, W.L., Hutson, W.H., Williams, D.F., Bé, A.W.H., Geitzenauer, K., Molfino, B., 1980. Surface circulation of the Indian ocean during the last glacial maximum, approximately 18,000 years B.P. Quat. Res. 14, 309–336.

Prell, W.L., Marvil, R.E., Luther, M.E., 1990. Variability in upwelling fields in the northwestern Indian Ocean 2, data-model comparison at 9000 years B.P. Paleoceanography 5, 447–457.

Ramaswamy, V., Nair, R.R., 1994. Fluxes of material to the Arabian Sea and Bay of Bengal-sediment trap studies. Proc. Indian Acad. Sci. (Earth Planet. Sci.) 103, 189–210.

Rashid, H., Flower, B.P., Poore, R.Z., Quinn, T.M., 2007. A ~25 ka Indian Ocean monsoon variability record from the Andaman Sea. Quat. Sci. Rev. 26, 2586–2597.

Rashid, H., England, E., Thompson, L., Polyak, L., 2011. Late glacial to Holocene Indian summer monsoon variability based upon sediment records taken from the Bay of Bengal. Terr. Atmos. Ocean. Sci. 22, 215–228.

Raza, T., Ahmad, S.M., Sahoo, M., Banerjee, B., Bal, I., Dash, S., Suseela, G., Mukherjee, I., 2014. Hydrographic changes in the southern Bay of Bengal during the last ~65,000 y inferred from carbon and oxygen isotopes of foraminiferal fossil shells. Quat. Int. 333, 77–85.

Reichart, G.J., Lourens, L.J., Zachariasse, W.J., 1998. Temporal variability in the northern Arabian Sea oxygen minimum zone (OMZ) during the last 225000 years. Paleoceanography 13, 607–621.

Reichart, G.-J., Brinkhuis, H., Huiskamp, F., Zachariasse, W.J., 2004. Hyperstratification following glacial overturning events in the northern Arabian Sea. Paleoceanography 19, PA2013. https://doi.org/10.1029/2003PA000900.

Rosenthal, Y., Oppo, D.W., Linsley, B.K., 2003. The amplitude and phasing of climate change during the last deglaciation in the Sulu Sea, western equatorial Pacific. Geophys. Res. Lett. 30 (8), 1428. https://doi.org/10.1029/2002GL016612.
Sarma, V.V.S.S., Krishna, M.S., Viswanadham, R., Rao, G.D., Rao, V.D., Sridevi, B., Kumar, B.S.K., Prasad, V.R., Subbaiah, C.V., Acharyya, T., Bandopadhyay, D., 2013. Intensified oxygen minimum zone on the western shelf of Bay of Bengal during summer monsoon: influence of river discharge. J. Oceanogr. 69, 45–55.
Satpathy, R., Steinke, S., Singh, A.D., 2019. Monsoon-induced changes in surface hydrography of the eastern Arabian Sea during the early Pleistocene. Geol. Mag. 157 (6), 1001–1011. https://doi.org/10.1017/S0016756819000098.
Sautter, L.R., Thunell, R.C., 1991. Seasonal variability in $\delta^{18}O$ and $\delta^{13}C$ of planktonic foraminifera from an upwelling environment: sediment trap results from the San Pedro Basin, Southern California Bight. Paleoceanography 6, 307–334.
Schlitzer, R., 2014. Ocean Data View. http://odv.awi.de.
Schott, F., McCreary, J.P., 2001. The monsoon circulation of the Indian Ocean. Prog. Oceanogr. 51, 1–123.
Schulte, S., Müller, P.J., 2001. Variations of sea surface temperature and primary productivity during Heinrich and Dansgaard-Oeschger events in the northeastern Arabian Sea. Geo-Mar. Lett. 21, 168–175.
Schulz, H., von Rad, U.V., Erlenkeuser, H., 1998. Correlations between Arabian Sea and Greenland climate oscillations of the past 110,000 years. Nature 393, 54–57.
Schulz, H., von Rad, U.V., Ittekkot, V., 2002. Planktic foraminifera, particle flux and oceanic productivity off Pakistan, NE Arabian Sea: modern analogues and application to the palaeoclimatic record. Geol. Soc. Lond., Spec. Publ. 195, 499–516.
Sengupta, D., Bharath Raj, G.N., Shenoi, S.S.C., 2006. Surface freshwater from Bay of Bengal runoff and Indonesian throughflow in the tropical Indian Ocean. Geophys. Res. Lett. 33, L22609.
Shakun, J.D., Burns, S.J., Fleitmann, D., Kramers, J., Matter, A., Al-Subary, A., 2007. A high-resolution, absolute-dated deglacial speleothem record of Indian Ocean climate from Socotra Island, Yemen. Earth Planet. Sci. Lett. 259, 442–456.
Shetye, S.R., Shenoi, S.S.C., Gouveia, A.D., Michael, G.S., Sundar, D., Nampoothiri, G., 1991. Wind-driven coastal upwelling along the western boundary of the Bay of Bengal during the southwest monsoon. Cont. Shelf Res. 11, 1397–1408.
Sijinkumar, A.V., Nath, B.N., Clemens, S., 2016. North Atlantic climatic changes reflected in the late Quaternary foraminiferal abundance record of the Andaman Sea, north-eastern Indian Ocean. Palaeogeogr. Palaeoclimatol. Palaeoecol. 446, 11–18.
Singh, A.D., Kroon, D., Ganeshram, R.S., 2006. Productivity and OMZ intensity variation in the eastern Arabian Sea at the millennial scale. J. Geol. Soc. India 68, 369–377.
Singh, A.D., Jung, S.J.A., Darling, K., Ganeshram, R.S., Ivanochko, T., Kroon, D., 2011. Productivity collapses in the Arabian Sea during glacial cold phases. Paleoceanography 26, PA3210.
Singh, A.D., Jung, S.J.A., Anand, P., Kroon, D., Ganeshram, R.S., 2018. Rapid switch in monsoon-wind induced surface hydrographic conditions of the eastern Arabian Sea during the last deglaciation. Quat. Int. 479, 3–11.
Sinha, A., Berkelhammer, M., Stott, L., Mudelsee, M., Cheng, H., Biswas, J., 2011. The leading mode of Indian Summer Monsoon precipitation variability during the last millennium. Geophys. Res. Lett. 38, L15703.
Sirocko, F., Sarnthein, M., Erlenkeuser, H., Lange, H., Arnold, M., Duplessy, J.C., 1993. Century-scale events in monsoonal climate over the past 24,000 years. Nature 364, 322–324.
Southon, J., Kashgarian, M., Fontugne, M., Metivier, B., Yim, W.-S., 2002. Marine reservoir corrections for the Indian Ocean and Southeast Asia. Radiocarbon 44, 167–180.
Spezzaferri, S., Kucera, M., Pearson, P.N., Wade, B.S., Rappo, S., Poole, C.R., Morard, R., Stalder, C., 2015. Fossil and Genetic evidence for the Polyphyletic Nature of the Planktonic Foraminifera "*Globigerinoides*", and Description of the New Genus *Trilobatus*. PLoS One 10 (5), e0128108. https://doi.org/10.1371/journal.pone.0128108.
Spindler, M., Hemleben, C., Salomow, J., Smit, L., 1984. Feeding behaviour of some planktonic foraminifera in laboratory cultures. J. Foraminifer. Res. 14, 237–249.
Stoll, H.M., Arevalos, A., Burke, A., Ziveri, P., Mortyn, G., Shimizu, N., Unger, D., 2007. Seasonal cycles in biogenic production and export in Northern Bay of Bengal sediment traps. Deep-Sea Res. II Top. Stud. Oceanogr. 54 (5–7), 558–580.
Stuiver, M., Grootes, P.M., 2000. GISP2 Oxygen isotope ratios. Quat. Res. 53, 277–284. https://doi.org/10.1006/qres.2000.2127.
Stuiver, M., Reimer, P.J., 1993. Extended $^{14}C$ data base and revised CALIB 3.0 $^{14}C$ age calibration program. Radiocarbon 35 (1), 215–230.
Subramanian, V., 1996. The sediment load of Indian rivers - an update. In: Erosion and Sediment Yield: Global and Regional Perspectives, p. 236.
Tiwari, M., Ramesh, R., Somayajulu, B.L.K., Jull, A.J.T., Burr, G.S., 2005. Early deglacial (~19-17 ka) strengthening of the northeast monsoon. Geophys. Res. Lett. 32 (19), 1–4 [L19712]. https://doi.org/10.1029/2005GL024070.
Unger, D., Ittekkot, V., Schäfer, P., Tiemann, J., Reschke, S., 2003. Seasonality and interannual variability of particle fluxes to the deep Bay of Bengal: Influence of riverine input and oceanographic processes. Deep-Sea Res. II Top. Stud. Oceanogr. 50, 897–923.
Van Campo, E., Duplessy, J.C., Rossignol-Strick, M., 1982. Climatic conditions deduced from a 150 kyr oxygen isotope-pollen record from the Arabian Sea. Nature 296, 56–59.
Van der Zwaan, G.J., Jorissen, F.J., De Stigter, H.C., 1990. The depth dependency of planktonic/benthonic foraminiferal ratios: constraints and applications. Mar. Geol. 95, 1–16.
Vénec-Peyré, M.T., Caulet, J.P., 2000. Paleoproductivity changes in the upwelling system of Socotra (Somali Basin, NW Indian Ocean) during the last 72,000 years: evidence from biological signatures. Mar. Micropaleontol. 40, 321–344.
Vidya, P., Prasanna Kumar, S., 2013. Role of mesoscale eddies on the variability of biogenic flux in the northern and central Bay of Bengal. J. Geophys. Res. 118 https://doi.org/10.1002/jgrc.20423.
Vinayachandran, P.N., Yamagata, T., 1998. Monsoon response of the sea around Sri Lanka: Generation of thermal domes and anticyclonic vorticies. J. Phys. Oceanogr. 28, 1946–1960.
Vinayachandran, P.N., Murty, V.S.N., Ramesh Babu, V., 2002. Observations of barrier layer formation in the Bay of Bengal during summer monsoon. J. Geophys. Res. 107 (C12), SRF-19.
Wang, Y.J., Cheng, H., Edwards, R.L., An, Z.S., Wu, J.Y., Shen, C.-C., Dorale, J.A., 2001. A high-resolution absolute-dated late Pleistocene monsoon record from Hulu Cave, China. Science 294, 2345–2348.
Weber, M.E., Reilly, B.T., 2018. Hemipelagic and turbiditic deposits constrain lower Bengal Fan depositional history through Pleistocene climate, monsoon, and sea level transitions. Quat. Sci. Rev. 199, 159–173.
Weber, M.E., Lantzsch, H., Dekens, P., Das, S.K., Reilly, B.T., Martos, Y.M., Meyer-Jacob, C., Agrahari, S., Ekblad, A., Titschack, J., Holmes, B., 2018. 200,000 years of monsoonal history recorded on the lower Bengal Fan-strong response to insolation forcing. Glob. Planet. Chang. 166, 107–119.
Yuan, D.X., Cheng, H., Edwards, R.L., 2004. Timing, duration, and transitions of the last interglacial Asian monsoon. Science 304, 575–578.
Zhang, R., Delworth, T.L., 2005. Simulated Tropical Response to a Substantial weakening of the Atlantic Thermohaline Circulation. J. Clim. 18, 1853–1860. https://doi.org/10.1175/JCLI3460.1.
Zhang, R., Delworth, T.L., 2006. Impact of Atlantic multidecadal oscillations on India/Sahel rainfall and Atlantic hurricanes. Geophys. Res. Lett. 33 (17).
Zhou, X., Duchamp-Alphonse, S., Kageyama, M., Bassinot, F., Beaufort, L., Colin, C., 2020. Dynamics of primary productivity in the northeastern Bay of Bengal over the last 26,000 years. Clim. Past 16, 1969–1986. https://doi.org/10.5194/cp-2020-27.
Zorzi, C., Goñi, M.F.S., Anupama, K., Prasad, S., Hanquiez, V., Johnson, J., Giosan, L., 2015. Indian monsoon variations during three contrasting climatic periods: the Holocene, Heinrich Stadial 2 and the last interglacial-glacial transition. Quat. Sci. Rev. 125 (C), 50–60. https://doi.org/10.1016/j.quascirev.2015.06.009.